

Synoptic study of the seasonal variability of dust cases observed by the TOMS satellite over northern Saudi Arabia

Adel M. Awad¹ · Abdul-Wahab S. Mashat¹ · Ahmad O. Alamoudi¹ · Mazen E. Assiri¹

Received: 1 June 2014 / Accepted: 21 April 2015 / Published online: 6 May 2015
© Springer-Verlag Wien 2015

Abstract The aerosol index (AI) from the Total Ozone Mapping Spectrometer (TOMS) satellite and meteorological parameters from National Center for Environmental Prediction and the National Center for Atmospheric Research (NCEP/NCAR) reanalysis datasets were used to examine seasonal dust cases in northern Saudi Arabia. Considering all seasons, winter has the fewest dust cases, whereas summer has the most dust cases. Synoptically, surface high-pressure systems in the eastern and western regions are important for the occurrence of dust cases over the northern Arabian Peninsula. When the eastern high pressure prevails, the effects of the Indian low-pressure system on the Arabian Peninsula are weakened or become nonexistent. The extension of the western high-pressure system toward the southeast provides an opportunity for a low-pressure system over Southeast Africa to connect with the Indian low-pressure system, which increases the width of the low-pressure trough and affects the Arabian Peninsula by increasing the amount of dust over the region. At 850 hPa, the weather systems typically rotate clockwise between winter and autumn. In winter, cyclonic systems prevail in the northern region, while anticyclonic systems prevail in the south. The systems are oriented toward the northeast in spring, the west in summer, and the southeast in autumn. Moreover, northern cyclones at 500 hPa shrink as they move northward and the maximum wind speed at 250 hPa decreases from winter to summer. Furthermore, the case study confirms that a change in the relative strength of the pressure systems and a change in

the orientation of the isobars (contours) affect the amount of dust over the area. When the orientation of the isobar (contour) lines become strictly north to south or east to west, the amount of dust decreases and vice versa.

1 Introduction

The dust load in the atmosphere plays a major role in weather and climatic phenomena, especially via direct and semi-direct effects on the radiation budget, precipitation (Ramanathan et al. 2001; Kaufman et al. 2002), the tropical water cycle (Liepert et al. 2004), Asian monsoons (Lau and Kim 2006; Lau et al. 2006), West African monsoon (Lau et al. 2009; Sun et al. 2009), and atmospheric stability. In turn, the wind speed profile of the lower atmosphere is affected (Alizadeh Choobari et al. 2012).

Given the aforementioned importance of dust, it is valuable to examine *dust cases* that are characterized by an unusually high dust load over a specific area and time. Fortunately, the rapid progress in satellite monitoring of dust properties and the availability of meteorological datasets have enabled scientists to perform complete studies of specific global dust sources (Prospero et al. 2002; Washington et al. 2003), classify the source regions within a certain region (e.g., Arabian Peninsula) (Mashat and Awad 2010), and study the synoptic features that are associated with dust cases (e.g., Barnaba and Gobbi 2004; Papadimas et al. 2008; Hatzianastassiou et al. 2009; Gaetani and Pasqui 2012; Al-Jumaily and Ibrahim 2013; Awad and Mashat 2014; Awad et al. 2015).

Furthermore, many studies have assessed the relationship between dust loading in certain regions and associated synoptic and climate features. Specifically, many studies have examined the effect of the North Atlantic Oscillation (NAO) on the inter-annual variability of dust loads in the Mediterranean

✉ Adel M. Awad
amawad@kau.edu.sa; awad_adel@yahoo.com

¹ Department of Meteorology, King Abdul Aziz University, Jeddah, Saudi Arabia

basin (e.g., Moulin et al. 1997; Özsoy et al. 2001; Dayan et al. 2008). Moreover, Gkikas et al. (2012) revealed two frequent synoptic conditions that induce dust episodes; these conditions primarily occur in the Western Mediterranean and secondarily occur in the Central Mediterranean. The Western Mediterranean region of Europe is affected by the Azores anticyclone, while the Eastern Mediterranean is affected by a thermal low in Southwest Asia (primarily in summer). In the Central Mediterranean in spring and summer, anticyclonic conditions prevail over Central Europe and the East Atlantic Ocean, while low pressure affects the Mediterranean Basin and the Sahara. In addition, Awad and Mashat (2013) demonstrated the effects of the pressure gradient between the Azores high pressure and the thermal low-pressure systems located over the Arabian Peninsula on dust transport from deserts in Northeast Africa to Asia. Moreover, Hamidi et al. (2013) identified two primary synoptic categories of dust storms in northern Iran, i.e., the Shamal and frontal types. Furthermore, Al-Jumaily and Ibrahim (2013) identified the relationship between dust storms over Iraq and the development of a low-pressure system over Iran. Additionally, Awad et al. (2014) studied the synoptic patterns of spring dust cases in southwestern Saudi Arabia, which were identified using the aerosol index from the Total Ozone Mapping Spectrometer (TOMS) satellite. These authors found that the low-pressure system over the southern Arabian Peninsula deepens, subsequently forming a steep pressure gradient between the low-pressure system and the high-pressure system over the Arabian Sea.

Dust storms over Saudi Arabia are a very frequent phenomenon, and a better understanding of their spatial and temporal distributions is important. Therefore, the goal of this work is to study the seasonal distribution of dust cases over northern Saudi Arabia and to investigate the corresponding synoptic features using National Center for Environmental Prediction and the National Center for Atmospheric Research (NCEP/NCAR) meteorological data. The dust cases specified based on the number of grid points have aerosol index (AI) values measured from the TOMS satellite which satisfy a specific threshold value. This threshold value is described in the methodology sub-section.

The paper is organized as follows. In “Data and methodology” section, the data and methodology are described. “Results” section examines the statistical results and synoptic features of the seasonal composition of dust cases and the case study. The final section contains a discussion and conclusions.

2 Data and methodology

2.1 Data

Dust over land and water is detected using the AI measured with the TOMS satellite. The AI is defined as the difference

between backscattered radiation measured at two ultraviolet channels (i.e., 340 and 380 nm) (Herman et al. 1997; Torres et al. 1998). However, dust near the surface has a relatively weak TOMS AI response (Mahowald et al. 2003). To avoid this deficiency in the aerosol index, many researchers have used a threshold value. For example, Prospero et al. (2002) used varying thresholds with values of 1.0 over North Africa, the Middle East, and South and Central Asia and 0.7 over all other areas. Additionally, Gao and Washington (2009) used a threshold of 1.0 to identify dust activity in the TOMS AI values. In this study, an AI threshold is implemented as a condition for selecting cases; the magnitude of this threshold and its identification is discussed in the methodology sub-section.

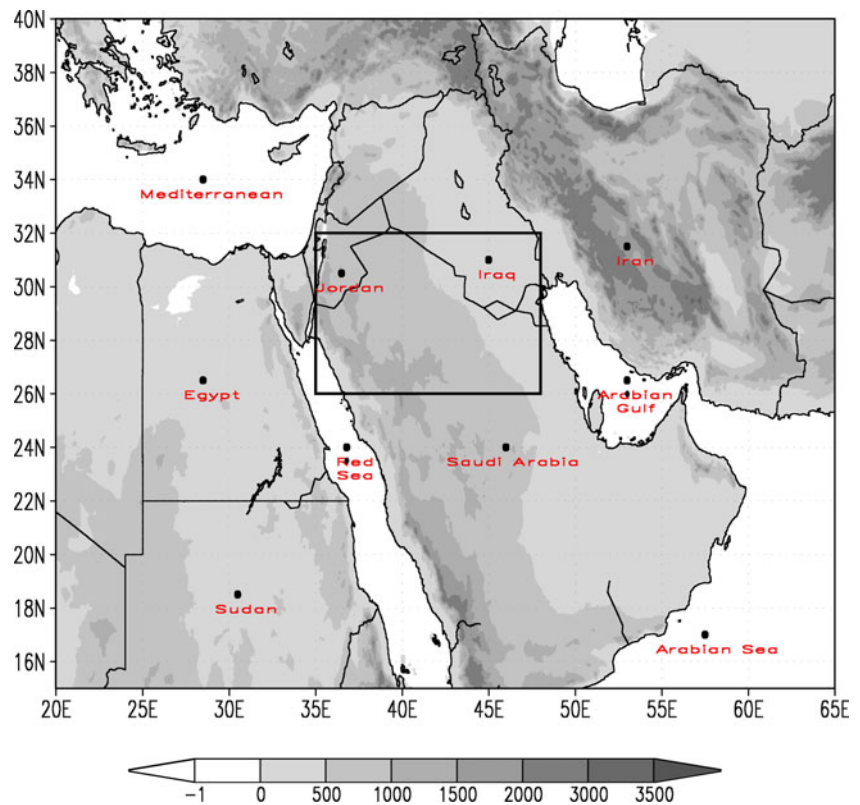
Twenty-five-year data were collected using four different TOMS instruments from November 1978 to 2006; a data gap exists from May 1993 to July 1996. It is worth noting that this dataset is consistent and adequate for the characterization of dust loading on a climatological basis (Kiss et al. 2007; Kalivitis et al. 2007; Li et al. 2009).

The meteorological data at 12 GMT (which corresponds to the closest TOMS observation time, i.e., approximately 12:00 local time) consist of monthly sea-level pressure (SLP), geopotential height, temperature, wind components from 1000 to 500 hPa, and wind components at 250 hPa from 1979 to 2006; these data are used for the synoptic assessment. The meteorological data are derived from the NCEP/NCAR reanalyses (Kalnay et al. 1996; Kistler et al. 2001) and have a spatial resolution of $2.5^\circ \times 2.5^\circ$ in the latitudinal and longitudinal directions. The study domain is defined by 30° – 62° E longitude and 10° – 45° N latitude. Additionally, the static stability is calculated and used for the diagnostic analysis and for describing the horizontal distribution of the stability for the seasonal and case study dust cases.

2.2 Methodology

In this study, dust cases were selected based on the magnitude (exceeding 1.7969, which is referred to as the threshold value) and extent (at least one grid point exceeding the predefined threshold) of the TOMS AI within the checking zone, which is delineated by 26° N to 32° N and 35° E to 48° E (Fig. 1). The threshold value represents the average aerosol index plus half of the standard deviation for all cases that had an aerosol index greater than zero for at least one grid point within the checking zone in spring. In this study, spring was selected as the mid-year season. Note that Barkan et al. (2005) used the average plus 1 standard deviation as a threshold value to determine dust days that affected Italy and Central Europe. Moreover, according to Prospero et al. (2002) and the OMTO3 readme file (2008) (available from the NASA Goddard Earth Sciences (GES) Data and Information Services Center (DISC), <http://disc.sci.gsfc.nasa.gov/>), the calculated threshold can be used for aerosol studies. Furthermore, the calculated threshold is

Fig. 1 A map representing the study domain (the *inside rectangle* represents the location of the checking zone and its location relative to the study domain)



comparable to other values used in the literature, e.g., those used by Awad and Mashat (2013) and Awad et al. (2014) to identify dust cases that move from Africa to Asia and dust cases over the southwestern Arabian Peninsula, respectively; those used by Prospero et al. (2002) to identify global dust sources; and those used by Barkan et al. (2004) to study dust intrusions over the Atlantic Ocean.

However, the checking zone has been classified as a secondary dust area of the Arabian Peninsula (Mashat and Awad 2010) and is considered a passage area for both spring Saharan cyclones (Hannachi et al. 2011) and Mediterranean wet season cyclones (Almazroui et al. 2014).

3 Results

The results focus on the general statistics and synoptic features of the seasonal dust cases and the seasonal synoptic features of an unusual year (2001–2002), which was selected as a case study.

3.1 Seasonal statistical study

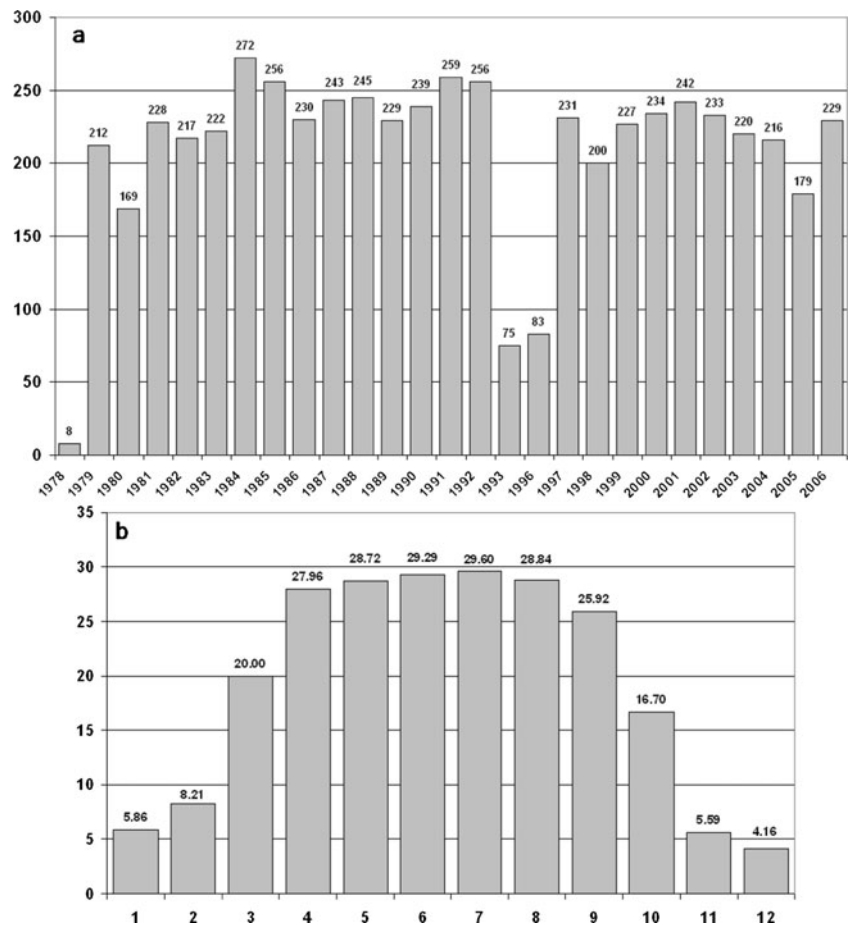
Applying the aforementioned method to the 1979–2006 data, with the exception of the data from November 1978 and from the period June 1993 to July 1996, 5654 dust cases (days) were identified. Excluding the incomplete years of 1978,

1993, and 1996, the average number of dust days per year was approximately 228.7 days. Thus, approximately 62.7 % of the year is dusty (Fig. 2a). Moreover, the monthly distribution of these cases (Fig. 2b) indicates that most of the dust cases occur in the warm months, i.e., from April to September. The cold months, especially from November to February, have the fewest cases; this result is similar to the findings of Li et al. (2009) for dust cases over the Arabian Peninsula.

In addition, the seasonal distribution of the selected cases (Table 1) shows that most cases occur in the summer and spring (approximately 72.2 % of cases), whereas few cases occur in winter (approximately 7.8 % of all cases) and a moderate number of cases occur in autumn (approximately 20 % of the cases). Additionally, Table 1 reveals that December and November have the fewest dust cases among all months, whereas July and August have the most dust cases. These results are consistent with those of Meloni et al. (2008) for the Central Mediterranean region, but inconsistent with the results of Dayan et al. (2008) and Gaetani and Pasqui (2012), who found that most dust events occur in spring in the Eastern Mediterranean region.

The seasonal distribution of dust cases (Fig. 3) shows that a high variability occurs among the winter seasons; however, this variability is relatively small among autumn seasons. In contrast, less variability exists among summer seasons, but the variability is still relatively high among the spring seasons. Additionally, it is noted that approximately 94.1 % of each

Fig. 2 a Annual and b monthly distributions of the selected dusty days for the period 1979 to 2006



summer season is dusty, whereas approximately 83.4 % of each spring season is dusty. In contrast, only 19.8 and 49.7 % of each winter and autumn, respectively, are dusty.

Furthermore, the horizontal distribution of AI in different seasons (Fig. 4) reveals that the AI increases from winter to summer before decreasing in autumn. Additionally, the distribution indicates several important concepts:

1. The eastern Arabian Peninsula has a high occurrence of dust cases, throughout the year. This area has been

previously identified as a global dust source (Prospero et al. 2002).

2. Both the northern shift and the relationship between dust over the Arabian Peninsula and Africa increase from winter to summer and begin to decrease in autumn, which is similar to the results of Prospero et al. (2002) and Washington et al. (2003).
3. Dust cases occur more often in spring than in autumn, even though both are transition seasons. This finding is consistent with the results of Meloni et al. (2008), especially because these dust cases satisfy their threshold values.

Table 1 Numbers and percentages of the selected dust events for different seasons and months

Season	Total, n (%)	Month 1, n (%)	Month 2, n (%)	Month 3, n (%)
Winter	444 (7.8)	79 (17.8)	131 (29.5)	234 (52.7)
Spring	1917 (33.9)	500 (26.1)	699 (36.5)	718 (37.4)
Summer	2164 (38.3)	703 (32.5)	740 (34.2)	721 (33.3)
Autumn	1129 (20.0)	648 (57.4)	384 (34.0)	97 (8.6)

The percentage of each distribution is shown within parentheses. The percentage of each season is calculated with respect to the total number of selected dust cases, and the percentage of each month is calculated according to the number of dust cases in the respective season. The total number of selected cases is 5654. The months of each season follow the traditional distribution of the seasons. For example, the winter months are December, January, and February

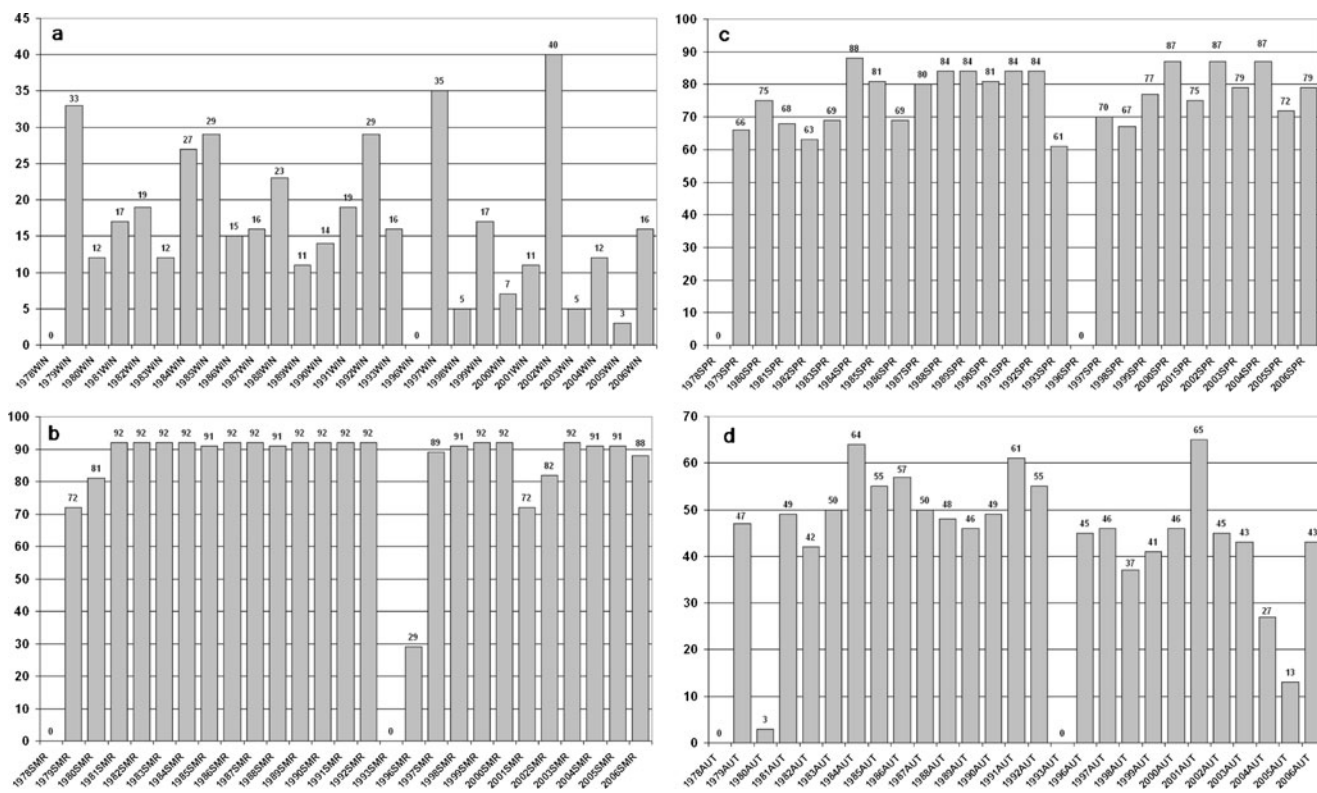


Fig. 3 The distributions of the selected dusty days in a winter, b summer, c spring, and d autumn from 1979 to 2006

3.2 Seasonal synoptic features

The synoptic features that correspond to the seasonal dust cases reveal the main features that differ among the seasons. Additionally, in our discussion, the synoptic description begins with a comparison of the synoptic features that are present in winter and summer, which are the seasons with the largest differences.

3.2.1 SLP and maximum wind at 250 hPa

The mean sea-level pressure for winter (Fig. 5(a)) reveals two high-pressure systems. The first system is centered over the western region, while the second system is centered over the northeastern region. Two low-pressure systems exist in the southern region. The first system is centered over Africa, while the second system is centered over India.

These systems affect the Arabian Peninsula via two high-pressure ridges and a low-pressure trough. The low-pressure trough extends northward from the African low pressure, while the two high-pressure ridges extend from the western high pressure, which affects the western Red Sea, and from the eastern high pressure, which affects the eastern Arabian Peninsula. In addition, the Indian low-pressure system affects the eastern Arabian Gulf via an extended low-pressure trough.

In summer (Fig. 5(b)), the northeastern wintertime high-pressure system becomes a component of the low-pressure system that is centered over India. Additionally, the Indian low-pressure system extends westward to form a low-pressure cell over the southeastern Arabian Peninsula and connects with the low-pressure system over Africa. Additionally, the Arabian Peninsula is affected by a broad low-pressure trough that extends from the newly formed low-pressure system, which has been previously shown to affect dust over the Eastern Mediterranean (Ganor et al. 2010).

In spring (Fig. 5(c)), the Indian summertime low-pressure system weakens and retreats eastward from Africa. Moreover, the low-pressure trough that affects the Arabian Peninsula in summer bifurcates into two branches that are separated by a high-pressure ridge that is an extension of the western high-pressure system. These two low-pressure troughs appear as though they extend from the low-pressure cell over the southeastern Arabian Peninsula and the low-pressure region over southeastern Africa. Additionally, it appears that the eastern wintertime high-pressure system remains; however, its strength is reduced.

In autumn (Fig. 5(d)), the pressure systems resemble those of summer; however, the systems tend to be weaker. Additionally, the low-pressure trough over the Arabian Peninsula begins to separate into two branches, which also

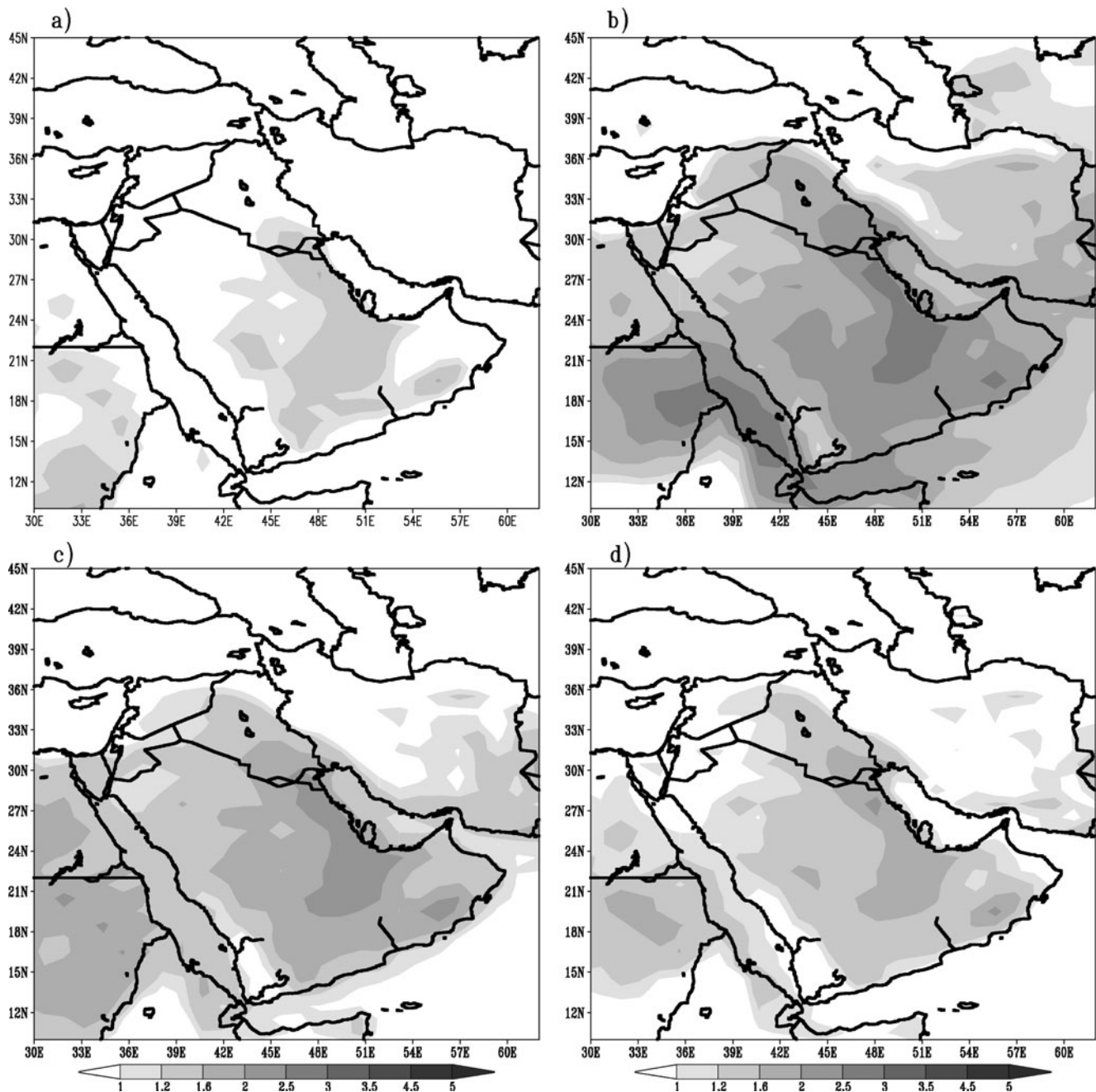


Fig. 4 Horizontal distribution of the aerosol index (dust) corresponding to *a* winter, *b* summer, *c* spring, and *d* autumn for the selected dusty days from 1979 to 2006

occurs in spring. Furthermore, the eastern high-pressure system begins to form in autumn.

It is clear that the relative positions of the high- and low-pressure systems and their strengths are important for determining the intensity of the dust cases. Similar results were found by Barkan and Alpert (2010), Awad and Mashat (2014), and Awad et al. (2014).

The seasonal distribution of the maximum wind at 250 hPa (Fig. 5) indicates that the strongest winds occur in winter (Fig. 5(a)), which is followed by spring (Fig. 5(c)), autumn (Fig. 5(d)), and a minimum in summer (Fig. 5(b)).

3.2.2 An 850-hPa pressure level and stability between 1000 and 850 hPa

In winter, the atmospheric conditions at 850 hPa (Fig. 6(a)) reveal that the northern area is affected by a cyclone, while the southern area is affected by an anticyclone. The cyclone impacts the western Arabian Peninsula via a cyclonic trough, while the eastern Arabian Peninsula is impacted by an anticyclonic ridge.

In summer (Fig. 6(b)), an anticyclonic system prevails over the western region and is centered over North Africa.

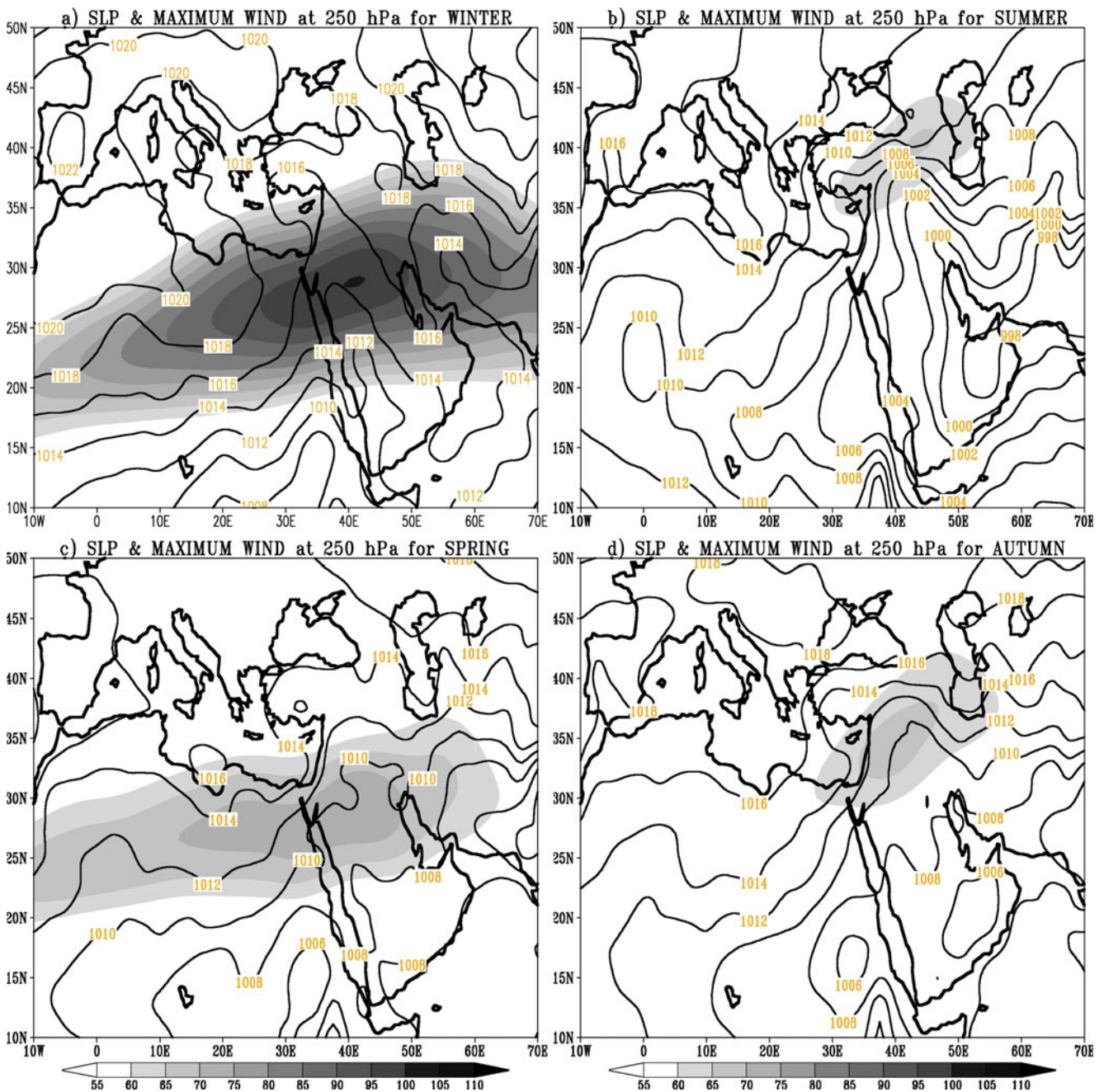


Fig. 5 Distribution of the mean sea-level pressure (SLP) (contours) and maximum 250-hPa wind speed (shaded) for a winter, b summer, c spring, and d autumn

Meanwhile, the eastern region is affected by a cyclonic system that is centered over India. The Arabian Peninsula is affected by a geopotential gradient between the anticyclonic and cyclonic systems. Additionally, the northern wintertime cyclone diminishes during the summer.

In spring, the atmospheric conditions at 850 hPa (Fig. 6(c)) reveal that the wintertime anticyclone over Africa shifts northeastward, while the anticyclonic cell over the Arabian Peninsula becomes smaller. Moreover, the northern wintertime cyclone weakens; its trough becomes smaller and moves northward.

In autumn (Fig. 6(d)), the African summertime anticyclone shifts eastward and produces an anticyclonic cell over the northeastern Arabian Peninsula. Moreover, the eastern summertime cyclone becomes weaker and shifts eastward to produce a weak geopotential gradient with the African anticyclone. Additionally, the northern cyclone, which forms in winter and dissipates in summer, begins to form again in autumn.

Based on the previous description, the cyclonic and anticyclonic systems are oriented west to east in winter, and their orientations begin to shift to north to south in spring. The systems reach their maximum strength while oriented north

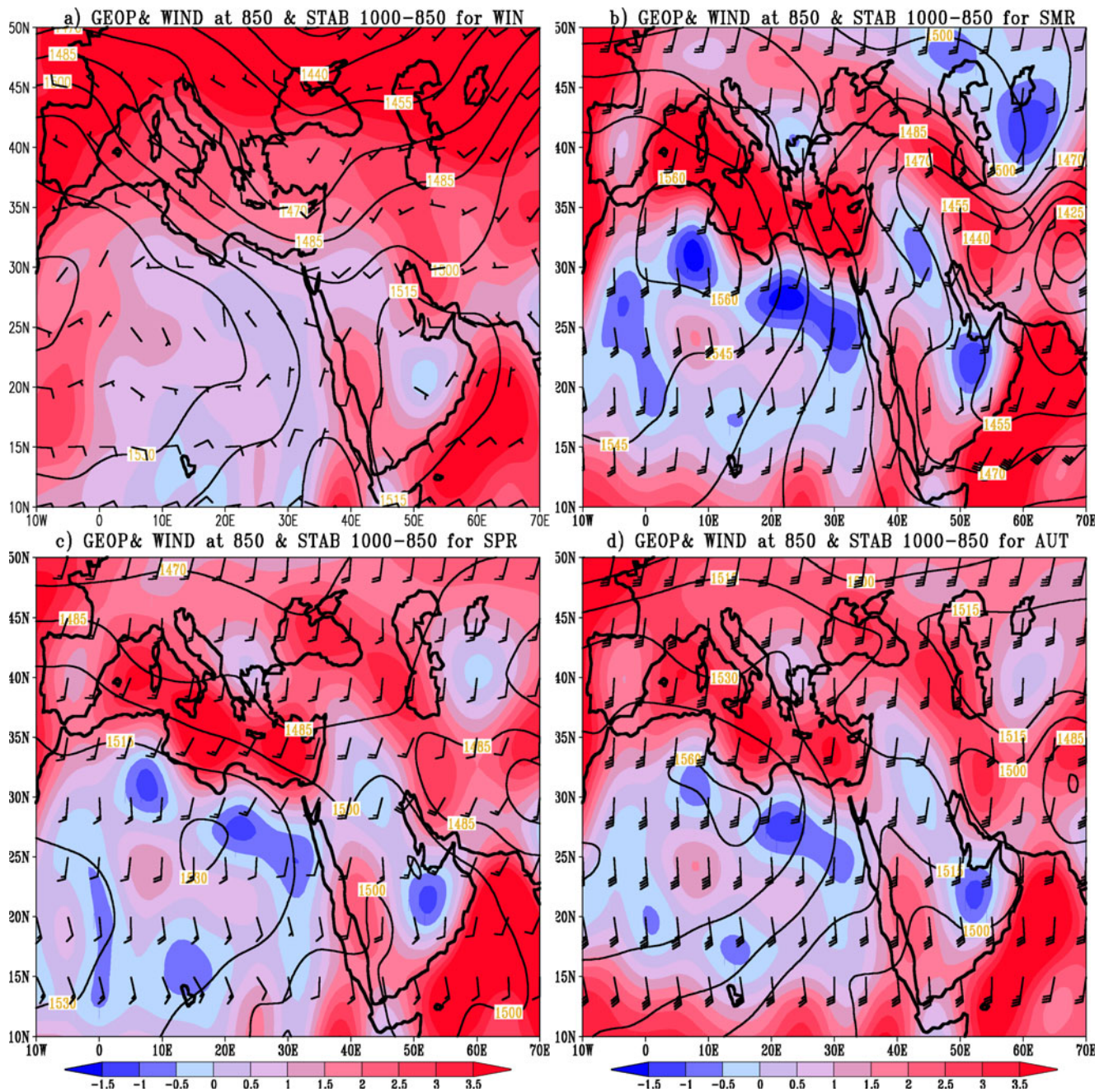


Fig. 6 Distribution of the geopotential (*contours*), the 850-hPa wind vectors (*barbs*), and the static stability between 1000 and 850 hPa (*shaded*) for *a* winter, *b* summer, *c* spring, and *d* autumn

to south in summer. Thereafter, the systems return to a west-to-east orientation in autumn. This seasonal distribution of the pressure systems is different from those found by Barkan and Alpert (2008) for dusty years over the Mediterranean, especially those in winter and summer.

Furthermore, winter has the weakest winds (Fig. 6(a)), whereas autumn has the strongest winds (Fig. 6(d)). However, the winds in spring (Fig. 6(c)) are relatively weak compared to the winds in summer (Fig. 6(b)).

The seasonal horizontal distribution of the variability in the static stability between 1000 and 850 hPa (Fig. 6) suggests that the unstable area over North Africa and over the eastern and northern portions of the Arabian Peninsula is surrounded by three regions of high stability: the Indian Ocean, the Mediterranean region, and the region east of the Arabian Gulf, which continues north to the Caspian Sea and the Black Sea.

However, each season has distinct characteristics. In winter (Fig. 6(a)), the instability in the atmospheric layer immediately above the Arabian Peninsula and North

Africa becomes weak. Moreover, the stable layers above the Mediterranean and East Arabian Gulf merge into one stable layer that encompasses the northern study region. Furthermore, the stable layer above the Indian Ocean weakens.

In contrast, although the distribution of stable and unstable areas in summer, spring, and autumn (Fig. 6(b–d), respectively) is similar, the unstable areas and the magnitude of the stability are largest in summer, which is followed by spring and autumn.

3.2.3 A 500-hPa pressure level and stability between 850 and 500 hPa

The atmospheric systems at 500 hPa are similar in all seasons (Fig. 7); i.e., a cyclonic system prevails over the north region, and an anticyclonic system prevails over the south region. However, specific characteristics for each season can be distinguished as a result of the interactions between the two systems. Specifically, the southern anticyclone shifts northward from winter (Fig. 7(a)) to summer (Fig. 7(b)) before shifting

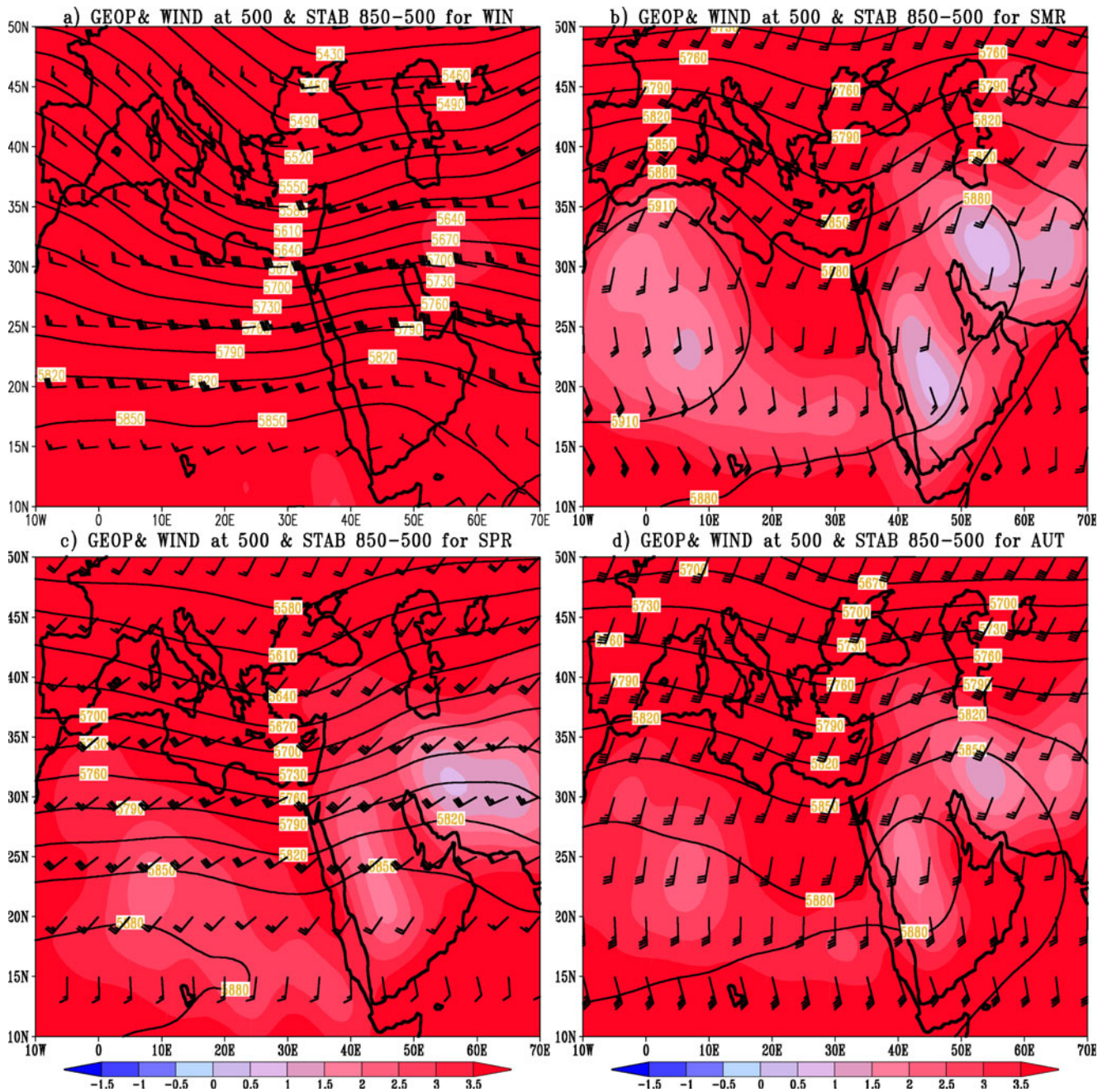


Fig. 7 Distribution of the geopotential (*contours*), 500-hPa wind vectors (*barbs*), and static stability between 850 and 500 hPa (*shaded*) for *a* winter, *b* summer, *c* spring, and *d* autumn

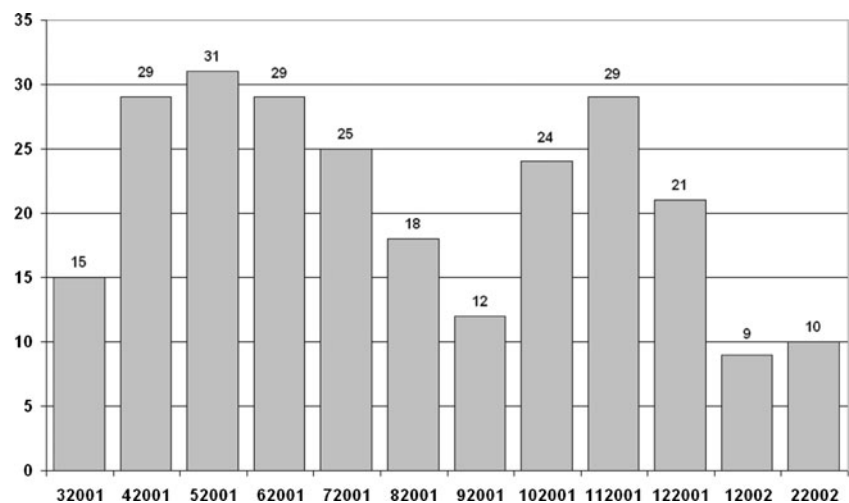
southward again in autumn (Fig. 7(d)). Additionally, the wind speeds decrease from winter to summer before increasing again in autumn. The cyclonic trough that affects Eastern Africa and the western Arabian Peninsula becomes deeper and more pronounced from winter to summer, reaching its greatest strength in summer (Fig. 7(b)). The cyclone begins to weaken in autumn. Additionally, the anticyclonic ridges that affect Africa and the Arabian Peninsula deepen from winter to summer; however, the ridges weaken again in autumn.

The wintertime horizontal distribution of the static stability variations between 850 and 500 hPa (Fig. 7(a)) indicates that the relatively less stable layers above the Arabian Peninsula and eastern Arabian Gulf are surrounded by layers of high stability over the northern study region, Africa, and the Arabian Sea. Similar stability distributions are found in the other seasons (Fig. 7(b–d)); however, the stability above the Arabian Peninsula, the eastern Arabian Gulf, and Africa is lower and reaches a minimum in summer (Fig. 7(b)). Furthermore, a new layer of lower stability appears during the summer over Western Africa and connects with the layer over the Arabian Peninsula. Lavaysse et al. (2009) and Calastrini et al. (2012) suggested that the stability of a dust-filled atmosphere could be interpreted by warming of the dust layer and cooling aloft; therefore, the previous results indicate that the dust layer is deeper in the warm months.

3.3 Synoptic features of the case study

A case study year was selected that satisfied the following conditions: it has a seasonal distribution that is different from the previous seasonal distribution, and it provides new information. The 2001–2002 time period best satisfied the conditions. This period has the most winter dust cases among the studied years; however, this period does not have the most summer dust cases among the warm seasons (Figs. 3 and 8).

Fig. 8 The monthly distribution of the case study for the period 2001–2002



3.3.1 Case study statistics

The number of dust events for each season in the case study year and the average over the entire period are shown in Table 2. These values indicate that the number of cases increased in winter and autumn, whereas they decreased in summer and spring. Additionally, the monthly distribution (Fig. 8) indicates that most cases occur in March and November, whereas the fewest cases occur in September and February. This result suggests that most dust cases occur during the transitional seasons rather than in summer.

A comparison of the horizontal seasonal distribution of dust for the case study year and the average values for the seasonal dust cases (Fig. 4) shows that more dust is present and that the dust extends northward in winter (Fig. 9(a)). However, in summer (Fig. 9(b)), the amount of dust is reduced and covers a smaller area. Additionally, in spring (Fig. 9(c)), the amount of dust is small; however, the area covered by dust is similar to the area covered in summer. In autumn (Fig. 9(d)), the northern extension and the connection between African and Arabian Peninsula dust are pronounced only in the north.

3.3.2 SLP and maximum wind at 250 hPa

In this section, the description of the synoptic features focuses on the seasonal difference between the case study year and the previous average seasonal synoptic features. In winter (Fig. 10(a)), the pressure increases within the eastern and northwestern high-pressure systems. The former high-pressure system extends southeastward, whereas the second system becomes smaller and retreats westward. In addition, the eastern low-pressure system deepens and shifts northwestward. This change causes an increase in the pressure gradient along the western side of Asia and around the Arabian Gulf. Moreover, the location of the maximum 250-hPa wind speed does not change; however, the actual value decreases.

Furthermore, the 250-hPa winds become oriented toward the northeast.

In summer (Fig. 10(b)), although the pressure within the eastern low-pressure system does not change, the area of low pressure increases over the Arabian Peninsula and shifts the contour lines to the south. In contrast, the pressure contours exhibit a north-south orientation. Simultaneously, the expansion of the western high pressure to the Mediterranean produces a relatively deep ridge over the northwestern Arabian Peninsula. Moreover, the emergence of a high-pressure cell northeast of the study region nudges the ridge that is located to the east of the eastern low-pressure trough toward the south. The relative positions of the ridge and trough redirect the low-pressure trough toward a straighter north-south orientation. In addition, the maximum 250-hPa wind speed is relatively weak and easterly. All of these changes combine to move the pressure gradient area to the east of the Arabian Peninsula and create a barrier between northeastern Africa and the northern Arabian Peninsula.

In spring (Fig. 10(c)), the eastern low-pressure system and its extension over the Arabian Peninsula deepen, the pressure within the western high-pressure system increases, and strength of the northeastern high-pressure system decreases. As a result, the ridge of western high pressure becomes oriented to the southwest, which causes the isobars over northeastern Africa to become more northerly, while the associated secondary ridge (observed in winter) over the northwestern Arabian Peninsula becomes smaller and moves northward. In addition, the northern ridge that affects the Arabian Gulf becomes smaller and moves northward. Meanwhile, the maximum 250-hPa wind speed becomes smaller, especially over the North Arabian Peninsula.

In autumn (Fig. 10(d)), the pressure increases within the weather systems. Over the Arabian Peninsula, the pressure contours appear as short waves that contain small high-pressure cells. Moreover, the northeastern high-pressure system strengthens, which forces the eastern low-pressure system and the low-pressure cell over the southern Arabian Peninsula to shift southward. Additionally, the ridge associated with the western high-pressure system moves eastward and forces the low-pressure system over southeastern Africa to form a steep trough over the Red Sea. The pressure isobars over the

northwestern Arabian Peninsula also become reoriented in a northeasterly direction. Furthermore, the maximum 250-hPa wind speed decreases and its location shifts southward.

3.3.3 An 850-hPa pressure level and stability between 1000 and 850 hPa

The main differences in winter (Fig. 11(a)) are an increase in the geopotential height of the anticyclonic systems in the eastern and western regions and a decrease in the geopotential height of the northern cyclone. The trough associated with the northern cyclone forms to the west, while the ridge associated with the southeastern anticyclone forms to the east.

These changes position the contours over the Arabian Peninsula to the south and increase the geopotential gradient over the Mediterranean. Furthermore, the wind speeds at this level decrease in all seasons.

In summer (Fig. 11(b)), the geopotential of the western anticyclone increases, while a new anticyclonic cell forms in the northeast region. Therefore, the eastern cyclone contours are pushed southward to form a deep ridge that subsequently reorients the contours over the eastern Arabian Peninsula to a more northerly direction. Simultaneously, the effect of the ridge associated with the western anticyclone over the Arabian Peninsula produces wavy contours over the peninsula.

In spring (Fig. 11(c)), the geopotential decreases for the eastern and northern cyclones, increases for the western anticyclone, and decreases for the anticyclonic cell over the Arabian Peninsula. Moreover, the ridge of the western anticyclone migrates eastward, while the anticyclonic cell over the Arabian Peninsula extends northward, which shifts the northern trough northward and increases the geopotential gradient over the Arabian Gulf.

In autumn (Fig. 11(d)), the western anticyclone invades the Arabian Peninsula, which connects with the anticyclonic cell, while the eastern cyclone diminishes. The northern cyclone deepens, while its southern trough affects the northwestern Arabian Peninsula.

Furthermore, in winter (Fig. 11(a)), there is not a large difference (such as that between the dust cases and the seasonal distribution) in the distributions of stability and instability within the layer between 1000 and 850 hPa, except for an increase in the stability over the northeastern Arabian Gulf and a decrease in the instability over the Mediterranean and northern Arabian Peninsula. In the other seasons (Fig. 11(b–d)), the unstable areas become smaller, while the stable areas expand.

3.3.4 A 500-hPa pressure level and stability between 850 and 500 hPa

The differences above the 500-hPa pressure level are as follows: in winter (Fig. 12(a)), only a slight difference is observed, and the cyclonic trough over the western Arabian

Table 2 The seasonal average numbers and percentages of the selected dust events

Season	Average for the entire period, n (%)	Case study year, n (%)
Winter	17.8 (19.8)	40 (54.4)
Spring	76.7 (83.4)	75 (81.5)
Summer	86.6 (94.1)	72 (78.3)
Autumn	45.2 (49.7)	65 (71.4)

Each average is calculated from the total number of cases with respect to the total number of days during the study period. The percentage of each distribution is shown within parentheses. The percentage of each season is calculated with respect to the total number days in each season

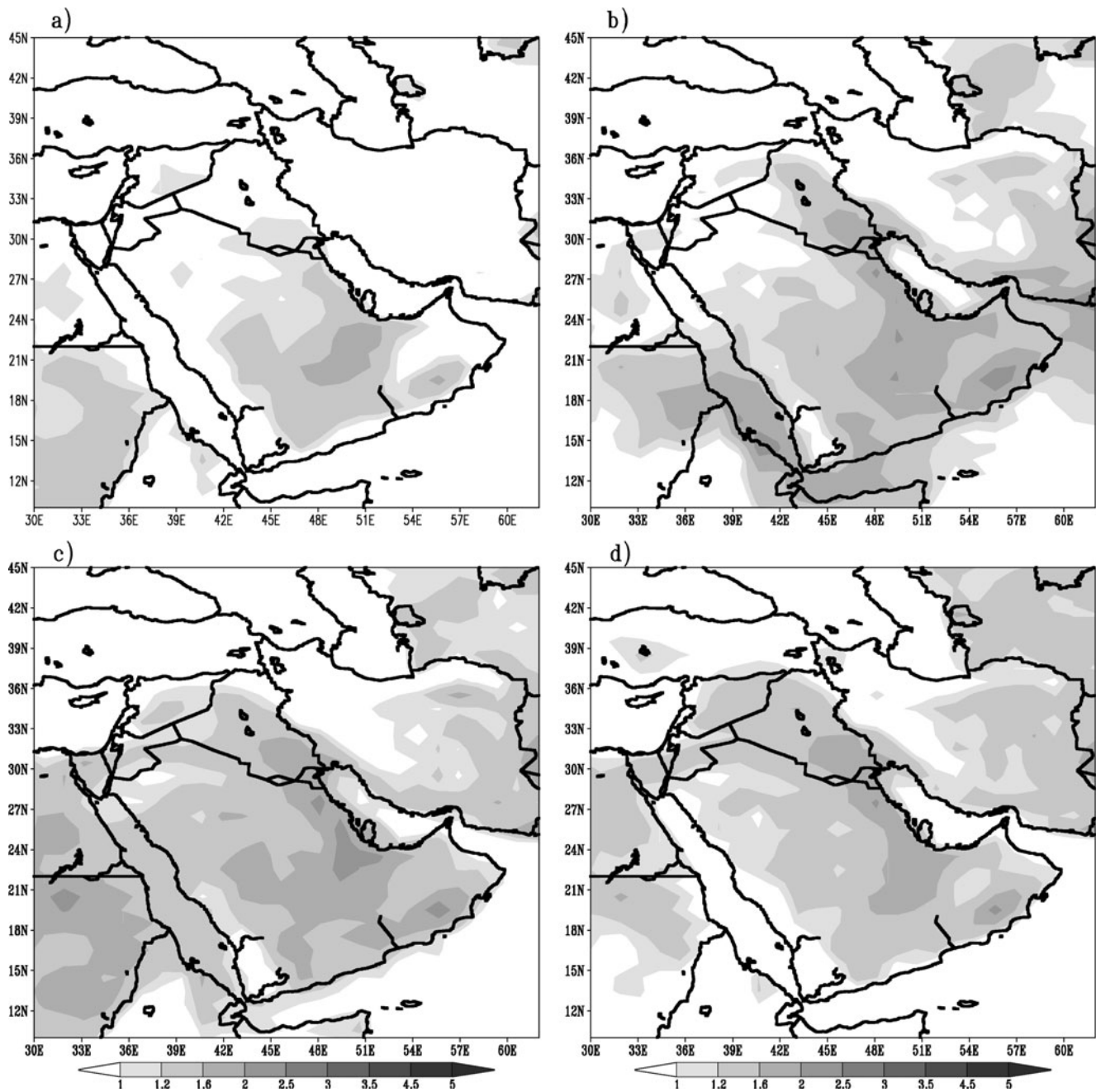


Fig. 9 Horizontal distribution of the aerosol index (dust) corresponding to *a* winter, *b* summer, *c* spring, and *d* autumn for 2001–2002 (i.e., the case study year)

Peninsula is deeper. In summer (Fig. 12(b)), the geopotential height of the western anticyclone increases and forms a deep ridge over Western Europe, which shifts the northern cyclonic trough to the west. In spring (Fig. 12(c)), no pronounced changes occur except for the deepening of the ridge over the eastern Arabian Peninsula and of the trough over the western Red Sea. In autumn (Fig. 12(d)), the southern anticyclone becomes smaller and moves westward, while the trough over the western Arabian Peninsula becomes less pronounced. In general, the wind speed decreases in all seasons.

Furthermore, the stability within the layer between 850 and 500 hPa in winter over the southern Arabian Peninsula and Mediterranean Sea increases, while the stability decreases over the eastern Arabian Gulf (Fig. 12(a)). In summer (Fig. 12(b)), the stability decreases over the eastern Arabian Gulf, while the relatively unstable layer over the southwestern Arabian Peninsula becomes smaller; the stable area over the Mediterranean expands. In spring (Fig. 12(c)), the stability of the layer above the eastern Arabian Gulf and South Sahara decreases, while the relatively less stable layer around the Red

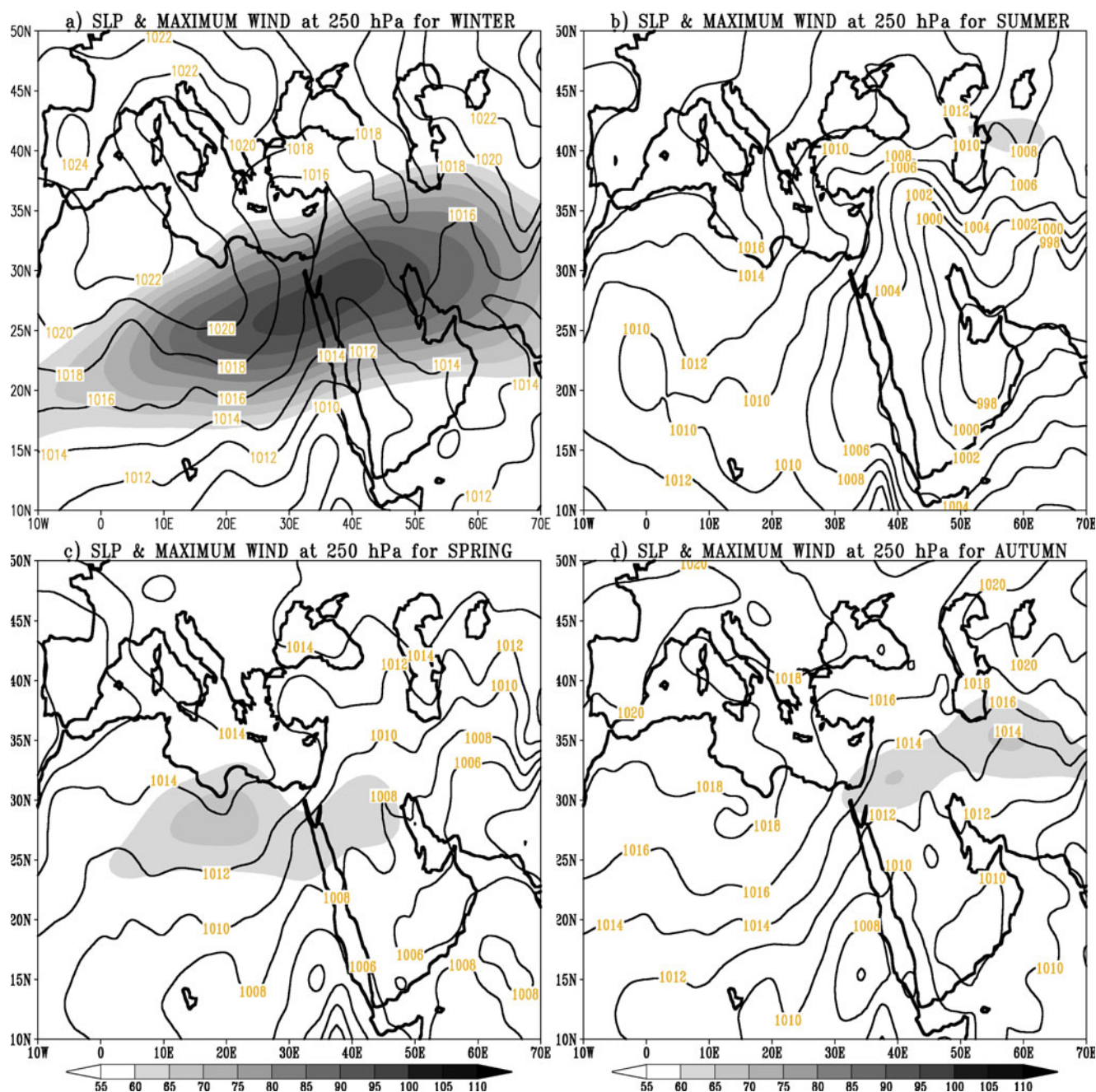


Fig. 10 Distribution of the mean sea-level pressure (SLP) (contours) and maximum 250-hPa wind speed (shaded) for a winter, b summer, c spring, and d autumn during the case study year

Sea expands; the stable layer over the Mediterranean Sea becomes smaller. In autumn (Fig. 12(d)), the stability increases over the entire area.

3.4 Anomaly study

The anomalies of geopotential height, relative to the seasonal climatology, at 850 hPa are shown in Fig. 13, for seasons, and Fig. 14, for cases studied. The statistical significance of compositions was calculated using *t* test (Wilks 1995), and the

regions where the seasonal compositions are statistically different from seasonal mean at the 99 % confidence level area are shaded. Also, for cases studied, the regions where the compositions are statistically different from seasonal mean at the 95 % confidence level area are shaded, except for the winter case study in which the shaded area is at the 90 % confidence level.

To better understand the details of the system, the seasonal anomalies of the geopotential height at 850 hPa have been studied. The winter anomaly, Fig. 13a, referred that the deepen and the south extend on northern cyclone are associated with

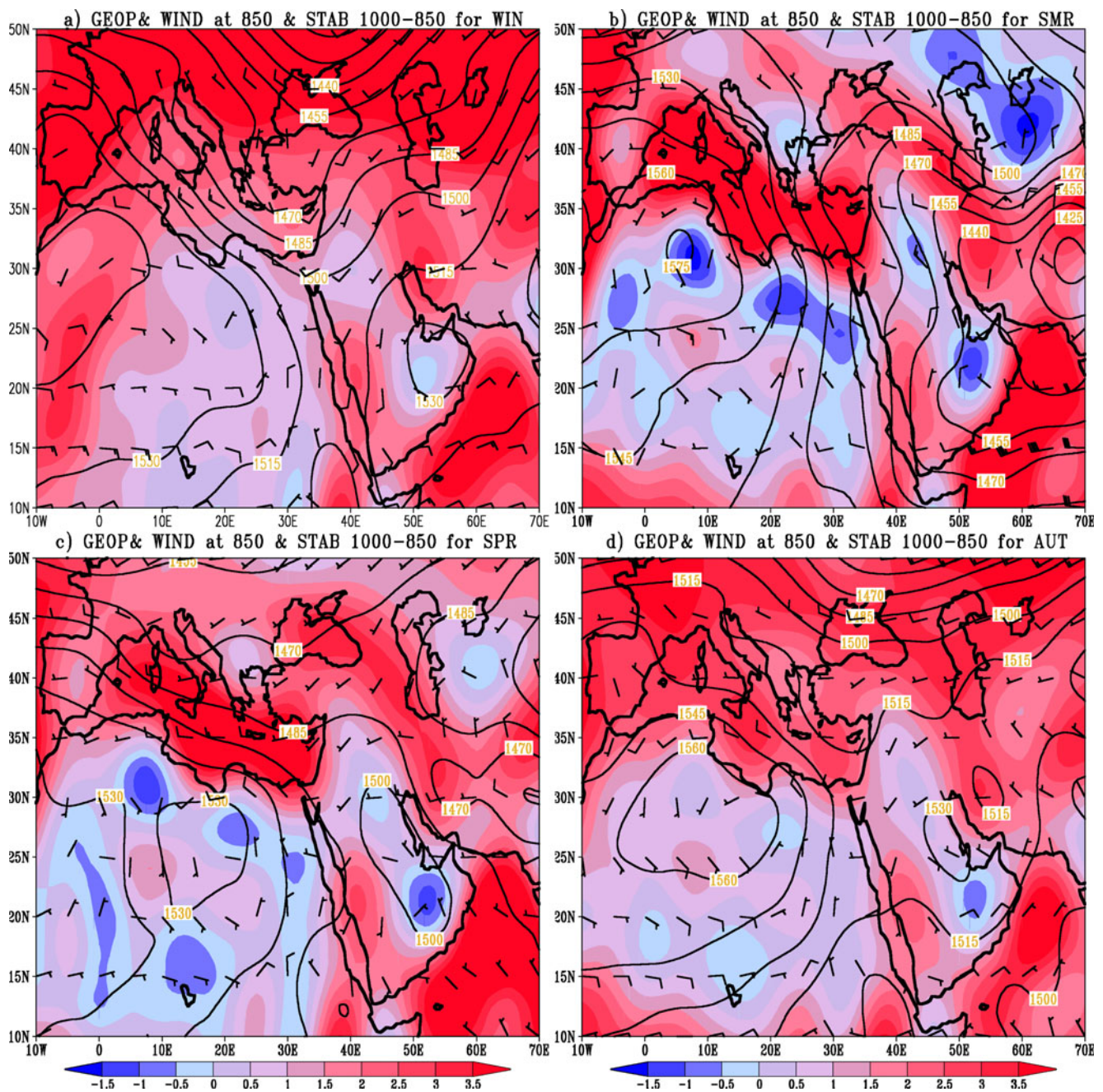


Fig. 11 Distribution of the geopotential (*contours*), 850-hPa wind vectors (*barbs*), and static stability between 1000 and 850 hPa (*shaded*) for *a* winter, *b* summer, *c* spring, and *d* autumn for the case study year

dust cases. However, the deepest anomaly is found in the northeast Mediterranean region. In the summer, the western anticyclone shifts eastward and the eastern cyclone weakens (Fig. 13b). These changes are meridional (oriented north-south) over the Arabian Peninsula. Likewise, the spring anomaly (Fig. 13c) exhibits relative deepening of the eastern cyclone and weakening of the northern cyclone. Additionally, an increase in strength and an eastward shift in the western anticyclone are associated with dust cases. In contrast, the increase in strength of the western anticyclone and the deepening of

the eastern cyclone represent the autumn anomaly changes of dust cases (Fig. 13d).

For the case study, the winter anomaly (Fig. 14a) involves a deeper northern cyclone over the Eastern Mediterranean and Red Sea, in addition to strengthening of the western and eastern anticyclones. Additionally, a strengthened western anticyclone and a relatively deep eastern cyclone, especially over the Arabian Peninsula and Eastern Mediterranean, are the main anomaly changes associated with the summer dust cases (Fig. 14b). Likewise, deeper anomalies for the northern and eastern cyclones and a stronger western anticyclone are

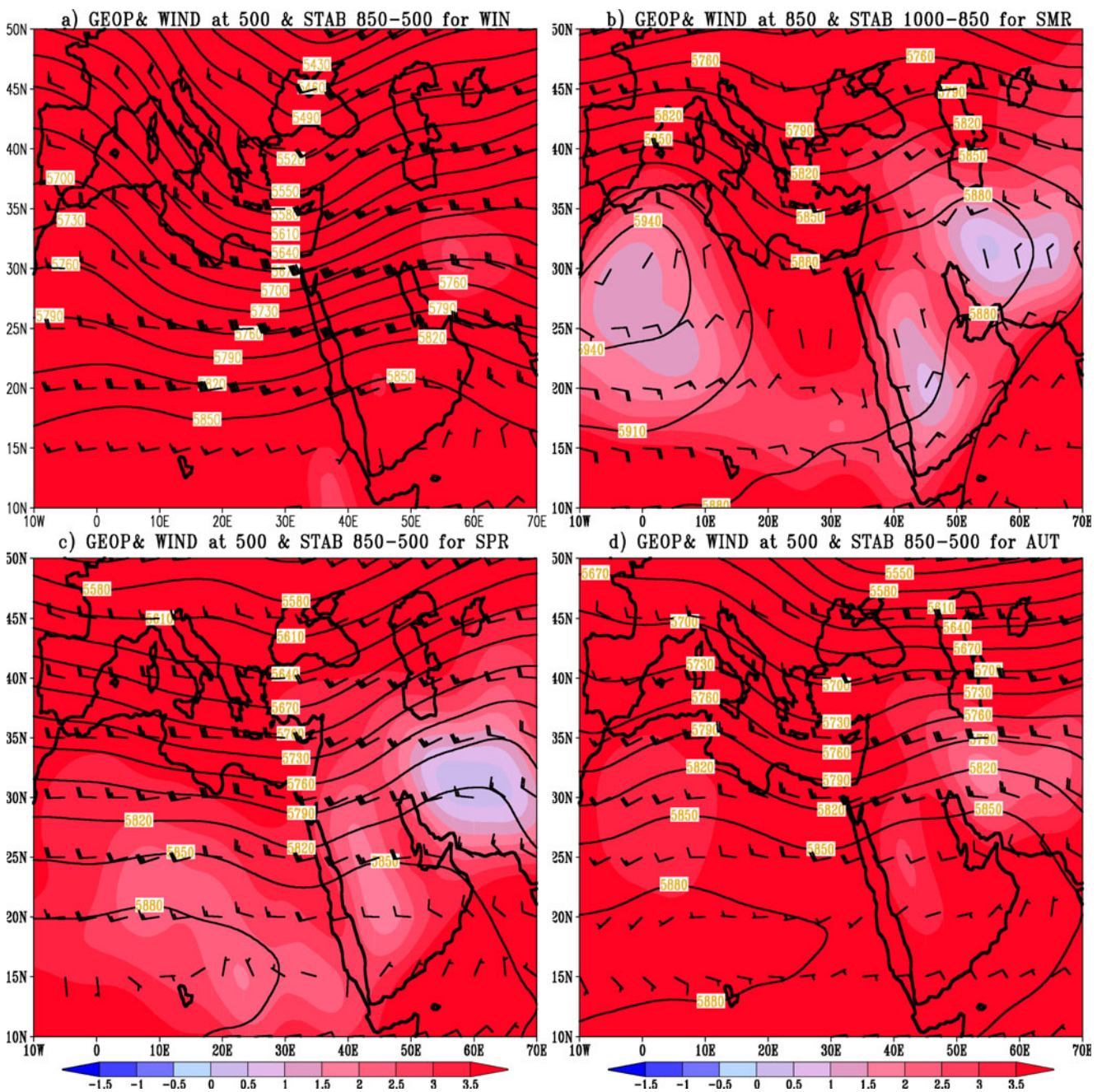


Fig. 12 Distribution of the geopotentials (*contours*), 500-hPa wind vectors (*barbs*), and static stability between 850 and 500 hPa (*shaded*) for *a* winter, *b* summer, *c* spring, and *d* autumn for the case study year

associated with the spring dust cases (Fig. 14c), whereas a strengthened southern anticyclonic area and deeper northern cyclone are the anomaly changes accompanying the autumn dust cases (Fig. 14d).

4 Discussion and conclusions

In this study, we examined the statistical and synoptic features that are associated with seasonal dust cases over northern

Saudi Arabia. The dust cases were classified based on the TOMS AI distribution and values. The TOMS AI data within the checking zone (delineated by 26° N to 32° N and 35° E to 48° E) were used to determine a threshold value of 1.7969.

By applying the threshold value to all years and seasons, it was found that northern Saudi Arabia is dusty for most of the year; however, most cases occur in the warm months, while only a few cases occur in the cold months. Specifically, July and August have the most dust cases, whereas November and December have the fewest dust cases.

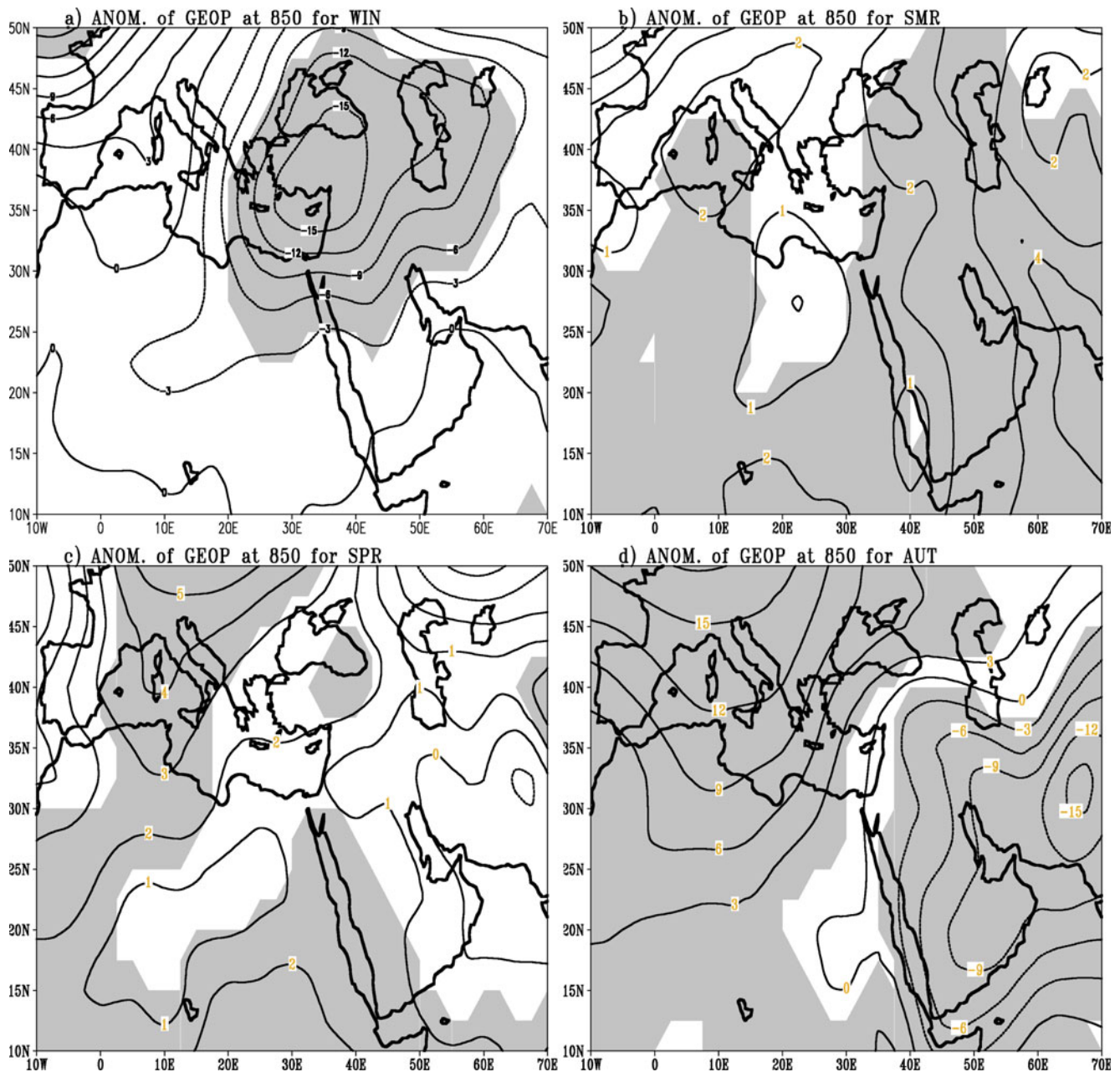


Fig. 13 Distribution of the geopotential anomaly at 850 hPa for **a** winter, **b** summer, **c** spring, and **d** autumn seasons. Anomalies within the shaded regions are statistically significant at the 99 % confidence level

From a synoptic perspective of the seasonal features, an important factor for dust over the northern Arabian Peninsula is the high-pressure systems over the eastern and western regions. The appearance of an eastern high-pressure system prevents the Indian low-pressure system from affecting the Arabian Peninsula (or at least weakens the effects). Ganor et al. (2010) also indicated the importance of high-pressure systems to dust over the Eastern Mediterranean. The northward and westward shift of the western high-pressure system increases the potential for the low-pressure system over southern Africa to develop and connect with the

Indian low-pressure system, which increases the width of the low-pressure trough that affects the Arabian Peninsula and increases the amount of dust over the region. Barkan et al. (2005) found that the strength and the relative position of the high- and low-pressure systems are the governing factors for generating dust events over the Central Mediterranean region.

An interesting synoptic feature at 850 hPa is the orientation of the atmospheric systems that spin clockwise from winter to autumn. The cyclonic and anticyclonic systems are oriented west to east in winter and partially west to east in spring, whereas they are oriented from south to north in summer

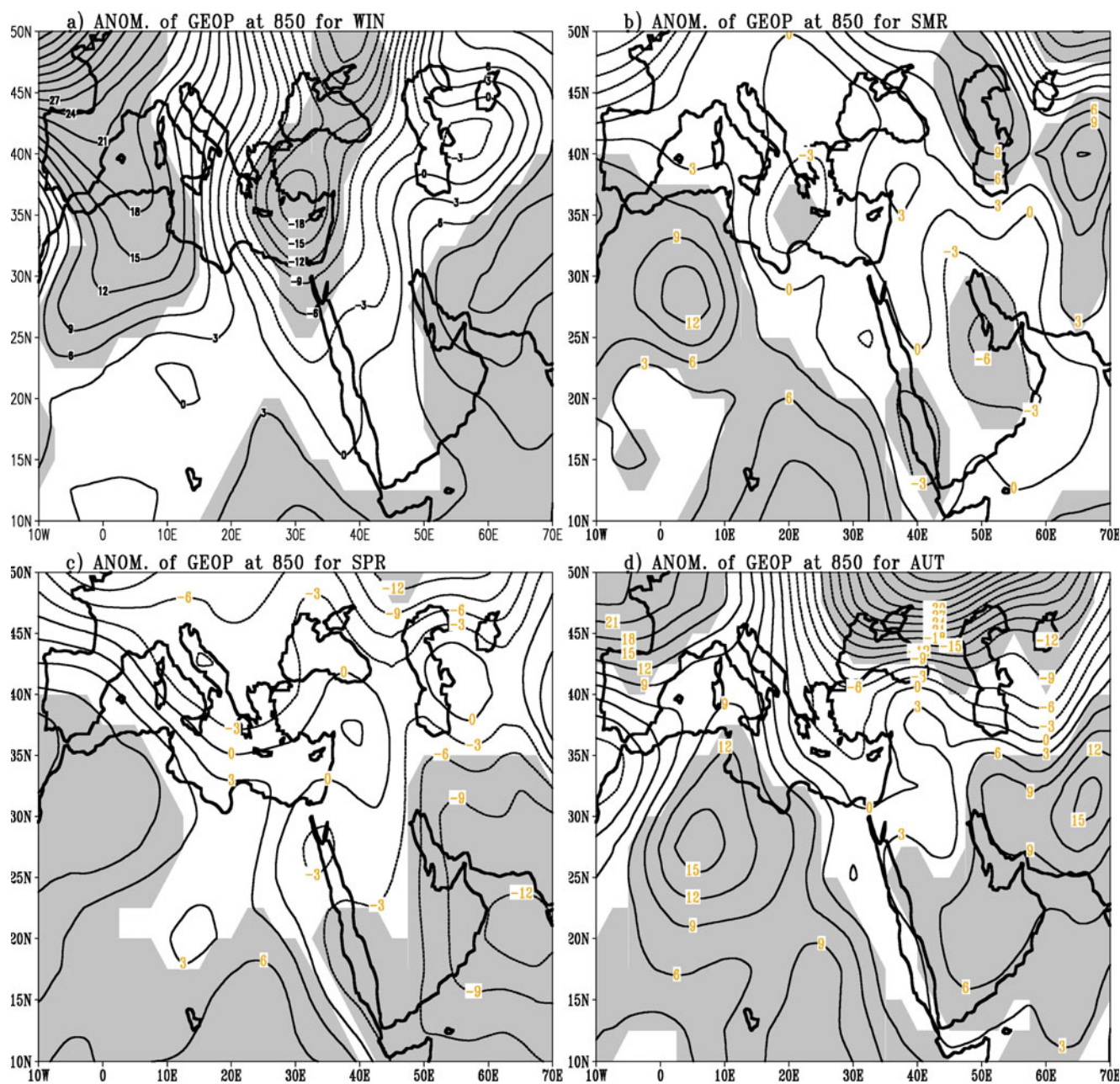


Fig. 14 Distribution of the geopotential anomaly at 850 hPa for **a** winter, **b** summer, **c** spring, and **d** autumn for the case study year. Anomalies within the shaded regions are statistically significant at the 95 % confidence level, except in winter in which it is statistically significant at the 90 % confidence level

and partially south to north in autumn. Additionally, the anomaly study demonstrated that the changes are mainly cyclonic in winter, anticyclonic in summer, and both cyclonic and anticyclonic in transition seasons.

The 850-hPa wind indicates that the wind speed increases from winter to autumn, reaching its minimum value in winter and its maximum value in autumn. In contrast, the 250-hPa winds attain their maximum in winter and minimum in autumn.

The static stability of the layer between 1000 and 850 hPa indicates that the unstable areas over North Africa and east

and north of the Arabian Peninsula are surrounded by three regions of high stability, i.e., over the southern Arabian Peninsula and Indian Ocean, over the Mediterranean Basin, and east of the Arabian Gulf to the Caspian Sea and the Black Sea. Additionally, the results suggest that the instability and stability of the atmospheric layers are higher in warm seasons; this result is similar to that found for desert depression (Thorncroft and Flocas 1997; Dayan et al. 2008) and dust cases over the eastern Arabian Peninsula (Awad et al. 2014).

The atmospheric systems at 500 hPa consist of a cyclonic system in the north and an anticyclonic system in the south.

However, the southern anticyclone shifts northward in warmer seasons, extended far to the north in summer; the anticyclone moves southward again in autumn. In addition, the cyclonic trough that affects Eastern Africa and the western Arabian Peninsula becomes deeper and more pronounced from winter to summer, reaching its maximum strength in summer. Furthermore, the 500-hPa wind speeds decrease from winter to summer and increase again in autumn.

Although the layer between 850 and 500 hPa is generally stable, the stability over the Arabian Peninsula and eastern Arabian Gulf is the lowest. Moreover, a new layer of lower stability forms over Western Africa in the warm season and reaches its minimum stability in summer. The unstable layer between 1000 and 850 hPa over the Arabian Peninsula and its effects on the stability between 850 and 500 hPa can be explained by the presence of low-level warm air and cold air aloft, which are associated with dust events (Lavaysse et al. 2009; Calastrini et al. 2012).

The pressure system distribution in the case study year demonstrates that when the high-pressure systems weakens, becomes smaller, and moves away from the Arabian Peninsula and when the low-pressure system over the eastern Arabian Peninsula does not deepen extensively, the amount of dust decreases. Additionally, the case study year confirms that the change in the orientation of the pressure (geopotential) contours causes a change in the amount of dust over the area. For example, when the contours are oriented north-south or west-east, the relationship between dust over Africa and the Arabian Peninsula weakens and vice versa. In addition, the increase in dust over the area is accompanied by weaker upper-level winds.

Acknowledgments The authors acknowledge the Deanship of Scientific Research, King Abdulaziz University, Jeddah, Saudi Arabia, for funding this study under grant number 486/155/1434. The authors also acknowledge the National Centers for Environmental Prediction (NCEP) and the National Center for Atmospheric Research (NCAR) for providing meteorological data and the National Aeronautics and Space Administration (NASA) for providing the TOMS data online.

References

- Alizadeh Choobari O, Zawar-Reza P, Sturman A (2012) Feedback between windblown dust and planetary boundary-layer characteristics: sensitivity to boundary and surface layer parameterizations. *Atmos Environ* 61:294–304. doi:10.1016/j.atmosenv.2012.07.038
- Al-Jumaily KJ, Ibrahim MK (2013) Analysis of synoptic situation for dust storms in Iraq. *Int J Energy Environ* 4(5):851–858
- Almazroui M, Awad AM, Islam MN, Al-Khalaf AK (2014) A climatological study: wet season cyclone tracks in the East Mediterranean region. *Theor Appl Climatol*. doi:10.1007/s00704-014-1178-z
- Awad AM, Mashat AS (2014) Synoptic features associated with dust transition processes from North Africa to Asia. *Arab J Geosci* 7(6):2451–2467. doi:10.1007/s12517-013-0923-4

- Awad AM, Mashat AS, Abo Salem FF (2015) Diagnostic study of spring dusty days over the southwest region of the Kingdom of Saudi Arabia. *Arab J Geosci*. doi:10.1007/s12517-014-1318-x
- Barkan J, Alpert P (2008) Synoptic patterns associated with dusty and non-dusty seasons in the Sahara. *Theor Appl Climatol* 94:153–162. doi:10.1007/s00704-007-0354-9
- Barkan J, Alpert P (2010) Synoptic analysis of a rare event of Saharan dust reaching the Arctic region. *Weather* 65:208–211
- Barkan J, Kutiel H, Alpert P (2004) Climatology of dust sources over the North African region, based on TOMS data. *Indoor Outdoor Environ* 13:407–419
- Barkan J, Alpert P, Kutiel H, Kishcha P (2005) Synoptics of dust transportation day from Africa toward Italy and central Europe. *J Geophys Res* 110, D07208. doi:10.1029/2004JD005222
- Barnaba F, Gobbi GP (2004) Aerosol seasonal variability over the Mediterranean region and relative impact of maritime, continental and Saharan dust particles over the basin from MODIS data in the year 2001. *Atmos Chem Phys* 4:2367–2391
- Calastrini F, Guarnieri F, Becagli S, Busillo C, Chiari M, Dayan U, Lucarelli F, Nava S, Pasqui M, Traversi R, Udisti R, Zipoli G (2012) Desert dust outbreaks over Mediterranean Basin: a modelling, observational and synoptic analysis approach. *Adv Meteorol* 2012, 246874. doi:10.1155/2012/246874
- Dayan U, Ziv B, Shoob T, Enzel Y (2008) Suspended dust over south-eastern Mediterranean and its relation to atmospheric circulations. *Int J Climatol* 28:915–924
- Gaetani, M., Pasqui, M., 2012. Synoptic patterns associated with extreme dust events in the Mediterranean Basin. *Reg Environ Change*, Springer, 1e14. <http://dx.doi.org/10.1007/s10113-012-0386-2>.
- Ganor E, Osetinsky I, Stupp A, Alpert P (2010) Increasing trend of African dust, over 49 years, in the eastern Mediterranean. *J Geophys Res* 115, D07201. doi:10.1029/2009JD012500
- Gao H, Washington R (2009) The spatial and temporal characteristics of TOMS AI over the Tarim Basin. *China Atmos Environ* 43(5):1106–1115. doi:10.1016/j.atmosenv.2008.11.013S
- Gkikas A, Houssos EE, Hatzianastassiou N, Papadimas CD, Bartzokas A (2012) Synoptic conditions favouring the occurrence of aerosol episodes over the broader Mediterranean Basin. *Q J Roy Meteorol Soc* 138:932–949. doi:10.1002/qj.978
- Hamidi M, Mohammad RK, Yaping S (2013) Synoptic analysis of dust storms in the Middle East. *Asia-Pac J Atmos Sci* 49(3):279–286
- Hannachi A, Awad A, Ammar K (2011) Climatology and classification of Spring Saharan cyclone tracks. *Clim Dyn* 37:473–491
- Hatzianastassiou N, Gkikas A, Mihalopoulos N, Torres O, Katsoulis BD (2009) Natural versus anthropogenic aerosols in the eastern Mediterranean Basin derived from multiyear TOMS and MODIS satellite data. *J Geophys Res* 114, D24202. doi:10.1029/2009JD011982
- Herman JR, Bhartia PK, Torres O, Hsu C, Seftor C, Celarier E (1997) Global distribution of UV-absorbing aerosols from Nimbus-7/TOMS data. *J Geophys Res* 102:911–916, 922
- Kalivitis N, Gerasopoulos E, Vrekoussis M, Kouvarakis G, Kubilay N, Hatzianastassiou N, Vardavas I, Mihalopoulos N (2007) Dust transport over the eastern Mediterranean derived from Total Ozone Mapping Spectrometer, Aerosol Robotic Network, and surface measurements. *J Geophys Res* 112(D3), D03202. doi:10.1029/2006JD007510
- Kalnay E, Kanamitsu M, Kistler R, Collins W, Deaven D, Gandin L, Iridell M, Saha S, White G, Woollen J, Zhu Y, Chelliah M, Ebisuzaki W, Higgins W, Janowiak J, Mo KC, Ropolewski C, Wang J, Leetma A, Reynolds R, Jenne R, Joseph D (1996) The NCEP/NCAR 40-year reanalysis project. *Bull Am Meteorol Soc* 77:437–471
- Kaufman YJ, Tanré D, Boucher O (2002) A satellite view of aerosols in the climate system. *Nature* 419:215–223

- Kiss P, Janosi IM, Torres O (2007) Early calibration problems detected in TOMS Earth-Probe aerosol signal. *Geophys Res Lett* 34, L07803
- Kistler R, Collins W, Saha S, White G, Woollen J, Kalnay E, Chelliah M, Ebisuzaki W, Kanamitsu M, Kousky V, vanden Dool H, Jenne R, Fiorino M (2001) The NCEP/NCAR 50-year reanalyses: monthly CD-ROM and documentation. *Bull Am Meteorol Soc* 82:247–267
- Lau K-M, Kim K-M (2006) Observational relationships between aerosol and Asian monsoon rainfall, and circulation. *Geophys Res Lett* 33, L21810. doi:10.1029/2006GL027546
- Lau KM, Kim MK, Kim KM (2006) Asian summer monsoon anomalies induced by aerosol direct forcing: the role of the Tibetan Plateau. *Clim Dyn* 26(7):855–864
- Lau KM, Kim KM, Sud YC, Walker GK (2009) A GCM study of the response of the atmospheric water cycle of West Africa and the Atlantic to Saharan dust radiative forcing. *Ann Geophys* 27(10):4023–4037
- Lavaysse C, Flamant C, Janicot S, Parker DJ, Lafore JP, Sultan B, Pelon J (2009) Seasonal evolution of the West African heat low: a climatological perspective. *Clim Dyn* 33:313–330
- Li J, Carlson BE, Laci AA (2009) A study on the temporal and spatial variability of absorbing aerosols using Total Ozone Mapping Spectrometer and Ozone Monitoring Instrument Aerosol Index data. *J Geophys Res* 114, D09213. doi:10.1029/2008JD011278
- Liepert BG, Feichter J, Lohmann U, Roeckner E (2004) Can aerosols spin down the water cycle in a warmer and moister world? *Geophys Res Lett* 31, L06207. doi:10.1029/2003GL019060
- Mahowald NM, Luo C, del Corral J, Zender C (2003) Interannual variability in atmospheric mineral aerosols from a 22-year model simulation and observation data. *J Geophys Res* 108. doi:10.1029/2002JD002821
- Mashat A, Awad AM (2010) The classification of the dusty areas over the Middle-East. *Bull Fac Sci Cairo Univ* 78(A):1–19
- Meloni D, di Sarra A, Monteleone F, Pace G, Piacentino S, Sferlazzo DM (2008) Seasonal transport patterns of intense Saharan dust events at the Mediterranean island of Lampedusa. *Atmos Res* 88(2):134–148
- Moulin C, Lambert CE, Dulac F, Dayan U (1997) Control of atmospheric export of dust from North Africa by the North Atlantic Oscillation. *Nature* 387:691–694
- Özsoy E, Kubilay N, Nickovic S, Moulin C (2001) A hemispheric dust storm affecting the Atlantic and Mediterranean in April 1994: analyses, modeling, ground-based measurements and satellite observations. *J Geophys Res* 106:18439–18460. doi:10.1029/2000JD900796
- Papadimas CD, Hatzianastassiou N, Mihalopoulos N, Kanakidou M, Katsoulis BD, Vardavas I (2008) Assessment of the MODIS Collections C005 and C004 aerosol optical depth products over the Mediterranean Basin. *Atmos Chem Phys* 9:2987–2999
- Prospero JM, Ginoux P, Torres O, Nicholson SE, Gill TE (2002) Environmental characterization of global sources of atmospheric soil dust identified with the Nimbus 7 total ozone mapping spectrometer absorbing aerosol product. *Rev Geophys* 40:2–31
- Ramanathan V, Crutzen PJ, Lelieveld J, Mitra AP, Althausen D, Anderson J, Andreae MO, Cantrell W, Cass GR, Chung CE, Clarke AD, Coakley JA, Collins WD, Conant WC, Dulac F, Heintzenberg J, Heymsfield AJ, Holben BN, Howell S, Hudson J, Jayaraman A, Kiehl JT, Krishnamurti TN, Lubin D, McFarquhar G, Novakov T, Ogren JA, Podgorny IA, Prather K, Priestley K, Prospero JM, Quinn PK, Rajeev K, Rasch P, Rupert S, Sadoumy R, Satheesh SK, Shaw GE, Sheridan P, Valero FPJ (2001) Indian Ocean experiment: an integrated analysis of the climate forcing and effects of the great Indo-Asian haze. *J Geophys Res* 106:28371–28398
- Sun DL, Lau WKM, Kafatos M, Boybeyi Z, Leptoukh G, Yang CW, Yang RX (2009) Numerical simulations of the impacts of the Saharan air layer on Atlantic tropical cyclone development. *J Clim* 22(23):6230–6250
- Thomcroft C, Flocas H (1997) A case study of Saharan cyclogenesis. *Mon Weather Rev* 125:1147–1165
- Torres O, Bhartia PK, Herman JR, Ahmad Z, Gleason K (1998) Derivation of aerosol properties from satellite measurements of backscattered ultraviolet radiation: theoretical basis. *J Geophys Res* 103:17099–17110
- Washington R, Todd M, Middleton MJ, Goudie AS (2003) Dust-storm source areas determined by the Total Ozone Monitoring Spectrometer and surface observations. *Ann Assoc Am Geogr* 93:297–313
- Wilks, D. S., 1995: *Statistical Methods in the Atmospheric Sciences—An Introduction*. International Geophysics Series, Vol. 59, Academic Press, 467 pp.